Steady state of a two-species annihilation process with separated reactants

Sasiri Juliana Vargas Urbano,[1,*] Diego Luis González,[1,†] and Gabriel Téllez[2,‡]
[1]*Departamento de Física, Universidad del Valle, A.A. 25360, Cali 760042, Colombia*
[2]*Departamento de Física, Universidad de los Andes, Bogotá 111711, Colombia*

(Received 4 March 2023; accepted 23 July 2023; published 10 August 2023)

We describe the steady state of the annihilation process of a one-dimensional system of two initially separated reactants A and B. The parameters that define the dynamical behavior of the system are the diffusion constant, the reaction rate, and the deposition rate. Depending on the ratio between those parameters, the system exhibits a crossover between a diffusion-limited (DL) regime and a reaction-limited (RL) regime. We found that a key quantity to describe the reaction process in the system is the probability $p(x_A, x_B)$ to find the rightmost A (RMA) particle and the leftmost B (LMB) particle at the positions x_A and x_B, respectively. The statistical behavior of the system in both regimes is described using the density of particles, the gap length distribution $x_B - x_A$, the marginal probabilities $p_A(x_A)$ and $p_B(x_B)$, and the reaction kernel. For both regimes, this kernel can be approximated by using $p(x_A, x_B)$. We found an excellent agreement between the numerical and analytical results for all calculated quantities despite the reaction process being quite different in both regimes. In the DL regime, the reaction kernel can be approximated by the probability to find the RMA and LMB particles in adjacent sites. In the RL regime, the kernel depends on the marginal probabilities $p_A(x_A)$ and $p_B(x_B)$.

DOI: 10.1103/PhysRevE.108.024118

I. INTRODUCTION

Reaction-diffusion (RD) systems are of great importance in modern physics due to their versatility as models for the study and description of many phenomena such as pattern formation, growth by aggregation, evolution of reactants by chemical reactions, disease spread, population growth, and opinion evolution [1–8].

In RD systems, the basic mechanism of matter transport is diffusion; once the interaction range is reached, the system components interact with each other through reactions. When the diffusion time is much longer than the reaction time, the system is said to be diffusion limited (DL); otherwise, it is said to be reaction limited (RL) [7–10]. In the DL regime, it is common to have spatial fluctuations in the density of reactants, which are translated into the nonhomogeneity of the system. In contrast, for the RL regime, the components are mixed, favoring the homogeneity of the system. The RD systems are generally difficult to study because they evolve through nonlinear processes out of equilibrium. Because of this, it is often necessary to use analytical approximations and numerical tools to describe the properties of the system.

Multispecies RD systems are quite interesting since the reactions occur in certain regions of the system where the concentrations of the reactants overlap. These regions are called "reaction zones" [2,11]. The description of the time evolution of these systems usually requires a proper understanding of the processes in the reaction zones as well as knowledge of the spatial distribution of particles in the reaction front. The RD systems with a two-species annihilation reaction

$$A + B \xrightarrow{\beta} \emptyset, \tag{1}$$

where $\emptyset$ is an empty site and β the reaction rate, have been widely studied since it is one of the simplest reactions that, in one dimension, can show anomalous kinetics [12,13]. This reaction has been used to describe the evolution of super-heavy magnetic monopoles produced in the very early universe. These monopoles evolve disappearing only through annihilation with an antimonopole [14]. Another example of the application of this reaction can be found in the study of epidemic reactions and epidemic spreading. In these cases, the contagion from one neighbor to the next is not always successful leading to a finite reaction rate as the one used in the current work. The particle-hole recombination in irradiated semiconductors is also a classical application of this reaction [15,16].

Recent studies focusing on reaction-diffusion systems on complex networks have shown how the topology of the underlying networks modify the statistical properties of the system [17–20]. For instance, for homogeneous networks with bounded fluctuations, the particle density decreases as the inverse of time. In contrast, for heterogeneous scale-free networks, the density decreases as a power law which depends on the degree distribution. There are other recent works about quantum reaction-diffusion dynamics that suggest that quantum effects change the collective universal behavior compared to that found in classical systems [21–24].

Another important factor in the time evolution of RD systems is the initial condition. In Refs. [14,25] the time evolution of a random mixture of reactants with the reaction

*sasiri.vargas@correounivalle.edu.co
†diego.luis.gonzalez@correounivalle.edu.co
‡gtellez@uniandes.edu.co

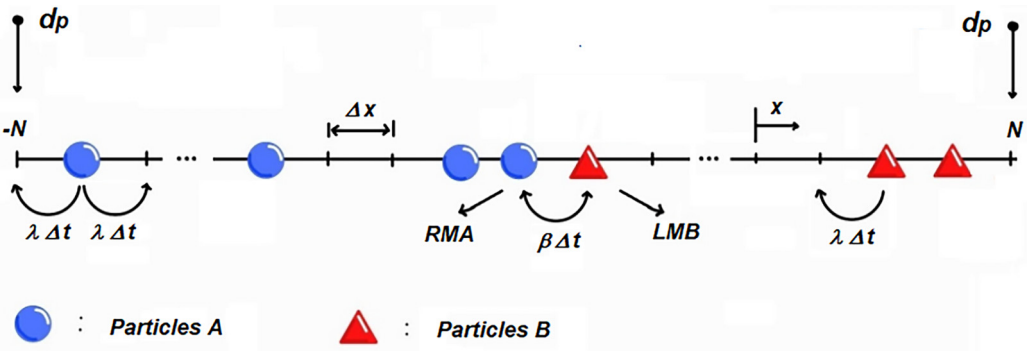

FIG. 1. Basic diagram of the processes that define the time evolution of the system. The hopping and reaction rates are λ and β, respectively. If one of the sites $i = \pm N$ is empty, the probability of deposition of a particle in that site is d_p.

given by Eq. (1) has been studied. Another initial condition that has been studied is that where the two types of reactants are initially separated [8,11,26–31].

The steady-state properties of a one-dimensional system of two reactants, A and B, initially separated into two well-defined spatial regions and subjected to the annihilation reaction given by Eq. (1), are studied in this paper to supplement the work presented in Ref. [11]. In the original work of Hoyuelos *et al.* [11], the statistical behavior of the system is described using numerical results for the density of reactants and complemented by numerical and analytical calculations for the gap length distribution between the particles A and B at the reaction front. In this paper we want to discuss a different approach to study the steady state of the system based on the calculation of a more fundamental quantity: the joint distribution for the positions of the rightmost A (RMA) and leftmost B (LMB) particles, $p(x_A, x_B)$. This distribution can be used not only to calculate $\mathcal{P}(\ell)$ but also the probability to have a reaction at position x and the probability to find the RMA and LMB particles at positions x_A and x_B, respectively. Unlike the work of Hoyuelos, we propose analytic expressions for the densities of particles A and B from the solution of a set of differential equations that depend on a reaction kernel. This kernel is estimated from the expression obtained for $p(x_A, x_B)$. Our analytical results are compared with those from numerical simulations. In contrast with the numerical algorithm proposed in Ref. [11], we use a rejection-free kinetic Monte Carlo (kMC) algorithm for our computer simulations.

II. SYSTEM DESCRIPTION

Following Ref. [11], a discrete one-dimensional lattice with $2N$ sites and two kinds of particles A and B is considered. At $t = 0$, all lattice sites are occupied in such a way that both species are separated into two independent regions: the particles A are in the lattice region $x < 0$, while the particles B are in the region $x > 0$. There are two types of interactions between particles. The first one is volume exclusion, i.e., each lattice site can be occupied at most by a single particle. The two-particle reaction given in Eq. (1) defines the second interaction. The probability that two adjacent particles A and B react in a time interval Δt is $p_r = \beta \Delta t$. Particles execute random hops in both directions exclusively to their empty nearest neighbors, moving a distance Δx in a time interval Δt. These hops occur with probability $\lambda \Delta t$, where λ is the hopping rate. The diffusion coefficient, D, can be calculated as $D = \lambda \Delta x^2$. On the other hand, at lattice sites, $i = -N$ and $i = N$, particles A and B are deposited, respectively. In this way there is an input of particles at each end of the lattice. The probability of deposition is d_p if the site $i = \pm N$ is empty; otherwise, it is zero. A scheme of the system and the processes associated with its evolution is shown in Fig. 1.

For suitable values of the parameters d_p, β, and λ, the system reaches a steady state where the average number of particles that get into the lattice $J \Delta t$ equals the average number of reactions, $R \Delta t$, where J is the particle flux and R the system reaction rate of the system. In the limit, $\beta \gg \lambda$ the time associated with the diffusion process is much larger than the reaction time. In this regime, the system is limited by diffusion (DL). In the opposite case, $\beta \ll \lambda$, the typical reaction time is much larger than that of diffusion, and the system is limited by reaction (RL). Note that in the DL regime, the timescale associated with the diffusion is much larger than that of the reaction; therefore, in this regime the analytical expressions do not depend on β. In the RL regime, the opposite occurs, and the behavior of the system does not depend on D. For the intermediate regime, the statistical behavior depends on the relative value of the three basic timescales associated with diffusion, reaction, and input of particles.

As shown in Ref. [11], the distance distribution between the particles RMA and LMB, $\mathcal{P}(\ell)$, is a key quantity for describing the steady state of the system. The functional form of $\mathcal{P}(\ell)$ strongly depends on the ratio between the parameters β, λ, and D. According to Ref. [11], for the steady state $\mathcal{P}(\ell)$ can be approximated by the continuous distribution

$$\mathcal{P}(\ell) \approx \frac{J}{2D} \ell e^{-J\ell^2/4D}, \tag{2}$$

in the DL regime, while in the RL regime we have

$$\mathcal{P}(\ell) \approx \frac{J}{k} e^{-J\ell/k}, \tag{3}$$

where k is the reaction constant defined as $k = \beta \Delta x$.

III. JOINT PROBABILITY DISTRIBUTION

Let n and m be the lattice sites occupied by the particles RMA and LMB, respectively. The master equation for the joint probability distribution $P_{n,m}(t)$ can be found using the interparticle distribution function method [7–10,32]. The

detailed derivation is shown in Appendix A, resulting in

$$\begin{aligned}\frac{dP_{n,m}(t)}{dt} &= -4\lambda P_{n,m}(t) + \lambda[P_{n+1,m}(t) + P_{n-1,m}(t)] \\ &+ \lambda[P_{n,m+1}(t) + P_{n,m-1}(t)] \\ &+ \lambda\,(P_{n,m}\mathcal{Q}_{n,m} - P_{n,m-1}\mathcal{Q}_{n,m-1}) \\ &+ \lambda\,(P_{n,m}\tilde{\mathcal{Q}}_{n,m} - P_{n+1,m}\tilde{\mathcal{Q}}_{n+1,m}) \\ &+ \sum_{k=n+1}^{m-2} P_{k,k+1}\,\mathcal{T}_{n,m,k}, \end{aligned} \tag{4}$$

where $\mathcal{Q}_{n,m}$, $\tilde{\mathcal{Q}}_{n,m}$, and $\mathcal{T}_{n,m,k}$ are conditional probabilities defined in (A5), (A6), and (A7). Unfortunately, even in the steady state, it is difficult to find an explicit expression for $P_{n,m}(t)$ from Eq. (4) due to the presence of the unknown probabilities $\mathcal{Q}_{n,m}$, $\tilde{\mathcal{Q}}_{n,m}$, and $\mathcal{T}_{n,m,k}$ associated with the configurations $\mathcal{C}_1$: $\overset{i}{\bullet}\circ\cdots\circ\overset{k}{\bullet}\overset{k+1}{\blacktriangle}\circ\cdots\circ\overset{j}{\blacktriangle}$ and $\mathcal{C}_2$: $\bullet\,\overset{i+1}{\bullet}\circ\cdots\circ\overset{j}{\blacktriangle}$. The gap length distribution, $\mathcal{P}_l$, can be calculated from $p_{i,j}(t)$ by taking the following relation into account:

$$\mathcal{P}_l(t) = \sum_{n=-\infty}^{m-1}\sum_{m=n+1}^{\infty} p_{m,n}(t)\,\delta_{l-(m-n)}. \tag{5}$$

Therefore, replacing Eq. (4) in Eq. (5) and evaluating the sums, it is possible to find

$$\begin{aligned}\frac{d\mathcal{P}_l(t)}{dt} &= -4\lambda\mathcal{P}_l + 2\lambda\mathcal{P}_{l+1} + 2\lambda\mathcal{P}_{l-1} \\ &+ 2\lambda(\mathcal{P}_l\mathcal{Q}_l + \mathcal{P}_l\tilde{\mathcal{Q}}_l - \mathcal{P}_{l-1}\mathcal{Q}_{l-1} - \mathcal{P}_l\tilde{\mathcal{Q}}_{l-1}) \\ &+ k\,\mathcal{P}_1\mathcal{T}_l, \end{aligned} \tag{6}$$

where the conditional probabilities $\mathcal{T}_l$ and $\mathcal{Q}_l$ are defined by

$$P_1\,\mathcal{T}_l = P(\bullet\overbrace{\circ\cdots\circ\bullet\blacktriangle\circ\cdots\circ}^{\ell+1}\blacktriangle) \tag{7}$$

and

$$\mathcal{P}_\ell\,\mathcal{Q}_l = P(\bullet\overbrace{\circ\cdots\circ}^{\ell-1}\blacktriangle\blacktriangle), \tag{8}$$

respectively. In this notation $P(\mathcal{C})$ is the probability to have the configuration $\mathcal{C}$, black dots and triangles represent particles A and B, respectively, and open dots represent empty sites. Using Eqs. (6) to (8) and taking the continuum space limit, $\Delta x\,l \to \ell$ and $\mathcal{P}_l(t) \to \mathcal{P}(\ell,t)$, we found

$$\begin{aligned}\frac{\partial\mathcal{P}(\ell,t)}{\partial t} &= 2D\,\frac{\partial^2\mathcal{P}(\ell,t)}{\partial\ell^2} + 2D\,Q(\ell,t)\,\frac{\partial\mathcal{P}(\ell,t)}{\partial\ell} \\ &+ 2D\,P(\ell,t)\,\frac{\partial Q(\ell,t)}{\partial\ell} + k\,\mathcal{P}(0,t)\,T(\ell,t). \end{aligned} \tag{9}$$

Following Ref. [11], Eq. (9) can be solved in the stationary state regime using the following approximations. First,

$$\begin{aligned}Q_n &= \frac{P(\bullet\overbrace{\circ\ldots\circ}^{n-1}\blacktriangle\blacktriangle)}{P(\bullet\circ\ldots\circ\blacktriangle)} \approx \frac{P(\bullet\overbrace{\circ\ldots\circ}^{n-1}\blacktriangle)\,\frac{P(\overset{n}{\blacktriangle}\overset{n+1}{\blacktriangle})}{P(\blacktriangle)}}{P(\bullet\underbrace{\circ\ldots\circ}_{n-1}\blacktriangle)} \\ &= \frac{P(\overset{n}{\blacktriangle}\overset{n+1}{\blacktriangle})}{P(\blacktriangle)} \approx \rho_{n+1}. \end{aligned} \tag{10}$$

In the continuum limit, the last equation can be approximated by

$$\mathcal{Q}(\ell) \approx \frac{J}{D}\frac{\ell}{2} + \mathcal{P}(0). \tag{11}$$

The conditional probability $\mathcal{T}(\ell)$ can be approximated in a similar way,

$$\begin{aligned}T_i &= \frac{P(\bullet\overbrace{\circ\ldots\circ\bullet\blacktriangle\circ\ldots\circ}^{i+1}\blacktriangle)}{P_1} \approx \frac{P(\bullet\overbrace{\circ\ldots\circ}^{i-1}\blacktriangle)P_1}{P_1} \\ &\approx P(\bullet\overbrace{\circ\ldots\circ}^{i-1}\blacktriangle), \end{aligned} \tag{12}$$

which can be written as

$$\mathcal{T}(\ell) \approx \mathcal{P}(\ell). \tag{13}$$

Replacing Eqs. (11) and (13) in Eq. (9) it is possible to show that

$$\frac{d^2\mathcal{P}(\ell)}{d\ell^2} + \frac{J}{2D}\left(\frac{2D}{k} + \ell\right)\frac{d\mathcal{P}(\ell)}{d\ell} + \frac{J}{D}\mathcal{P}(\ell) = 0, \tag{14}$$

with $\mathcal{P}(\infty) = 0$ and $\mathcal{P}(0) = J/k$ the associated boundary conditions. The last condition represents the balance between annihilation and deposition of particles at the steady state. As shown in Ref. [11], the solution of Eq. (14) is given by

$$\mathcal{P}(\ell) = \frac{J}{2D}\left(\ell + \frac{2D}{k}\right)\mathrm{e}^{-\frac{J\ell}{4D}\left(\ell+\frac{4D}{k}\right)}. \tag{15}$$

Notice that Eq. (15) reduces to Eq. (2) for $D/k \to 0$ (DL regime) and to Eq. (3) for $D/k \to \infty$ (RL regime).

In the continuum spatial limit, the positions of the RMA and LMB particles are $x_A \to n\Delta x$ and $x_B \to m\Delta x$, respectively. The continuum version of the joint probability $p_{n,m}$, $p(x_A, x_B)$ for the steady state can be estimated using the change of variables $\ell = x_B - x_A$ and $\kappa = (x_A + x_B)/2$. Note that κ and ℓ are the position of the center of mass and the distance between the RMA and LMB particles, respectively. Due to the symmetry of the system, the average of κ, $\langle\kappa\rangle$, must be zero. Furthermore, the distribution of κ should be close to a Gaussian distribution because the position of the center of mass evolves by simple random walk. We propose the approximation $\mathcal{P}(\ell,\kappa) \approx \mathcal{G}(\kappa)\mathcal{P}(\ell)$ where $\mathcal{G}(\kappa)$ denotes the probability distribution of the position of the center of mass. This approximation assumes that the stochastic variables κ and ℓ are independent, i.e., the position of the center of mass is independent of the gap length. A similar approximation cannot be made in the space of variables x_A and x_B because these variables are strongly correlated due to the condition $x_B > x_A$. As mentioned before, the position of the center of mass evolves by diffusion. As a result, we propose $\mathcal{G}(\kappa) = \sqrt{a/\pi}\exp(-a\kappa^2)$, and the joint distribution $\mathcal{P}(\ell,\kappa)$ can be written as

$$\mathcal{P}(\ell,\kappa) \approx \sqrt{\frac{a}{\pi}}e^{-a\kappa^2}\,\frac{J}{2D}\left(\ell + \frac{2D}{k}\right)\mathrm{e}^{-\frac{J\ell}{4D}\left(\ell+\frac{4D}{k}\right)}, \tag{16}$$

where $a = 1/(2\sigma^2)$ with σ^2 the variance of the distribution $\mathcal{G}(\kappa)$, which is a measure of the width of the reaction front. The joint probability for the positions of the RMA and LMB

particles, $p(x_A, x_B)$, can be extracted from $\mathcal{P}_c(\ell, \kappa)$; we found

$$p(x_A, x_B) \approx \int d\ell \int d\kappa \, \{\mathcal{P}(\ell, \kappa)\, \delta[\ell - (x_B - x_A)] \times \delta[2\kappa - (x_A + x_B)]\} = \frac{J}{2D}\sqrt{\frac{a}{\pi}}\left(\frac{2D}{k} + (x_B - x_A)\right) e^{-\frac{a}{2}(x_A^2 + x_B^2)} \times e^{-(x_B - x_A)^2\left(\frac{J}{4D} - \frac{a}{4}\right) - \frac{J(x_B - x_A)}{k}}, \tag{17}$$

with $-\infty < x_A \leqslant x_B < \infty$. Equation (17) provides a simple interpretation for the behavior in the steady state of the RMA and LMB particles in terms of an equivalent two-particle system in equilibrium. In this equivalent system, the effective interaction potential is given by

$$\vartheta(x_A, x_B) = \log\left[\frac{2D}{k} + (x_B - x_A)\right] - (x_B - x_A)\left[(x_B - x_A)\left(\frac{J}{4D} - \frac{a}{4}\right) + \frac{J}{k}\right] - \frac{a}{2}\left(x_A^2 + x_B^2\right). \tag{18}$$

The first two lines represent the interaction between the particles RMA and LMB, while the third one represents the interaction of these particles with an external field. The logarithmic term leads to a repulsive force due to the reaction, and the second term is an attractive interaction due to diffusion. The third term can be interpreted as an interaction with an external quadratic field that confines the particles. This field can be associated with the effective force applied by the left and right neighbors of the RMA and LMB particles, respectively. For small distances, the interaction between particles is dominated by the logarithmic term, while for large distances, the last two terms are the most relevant.

IV. DISCUSSION

In contrast with the numerical algorithm proposed in Ref. [11], we implement a rejection-free kMC algorithm based on three events: deposition of particles, annihilation, and diffusion [33–35]; for more information see Appendix B. In our simulations we use $\Delta t = 1$, $\lambda = 1/2$, and $d_p = 1$. In the plots, lines correspond to the analytical model and dots to kMC results.

In Fig. 2 the behavior of $\mathcal{P}(\ell)$ for three different values of β is shown. For $\beta = 0.95$ (square dots) the system is in the DL regime, while for $\beta = 0.01$ (triangular dots) the system is in the RL regime. Note that our approach allows us to recover the previous results found in Ref. [11]. In the RL regime, $\mathcal{P}(\ell)$ decays exponentially, while in the DL the right tail of the distribution is Gaussian. The repulsive force between the RMA and LMB particles vanishes at low reaction rates, and the balance between deposition and reaction implies $\mathcal{P}(0) = J/k > 0$. For instance, from Fig. 2, for $\beta = 0.1$ (circular dots) we have $P(0) \approx 0.34$ implying $J \approx 0.034$.

From the distribution $p(x_A, x_B)$ given by Eq. (17) the marginal distributions for the positions of the RMA and LMB particles, $p_A(x_A)$ and $p_B(x_B)$, can be calculated. By definition

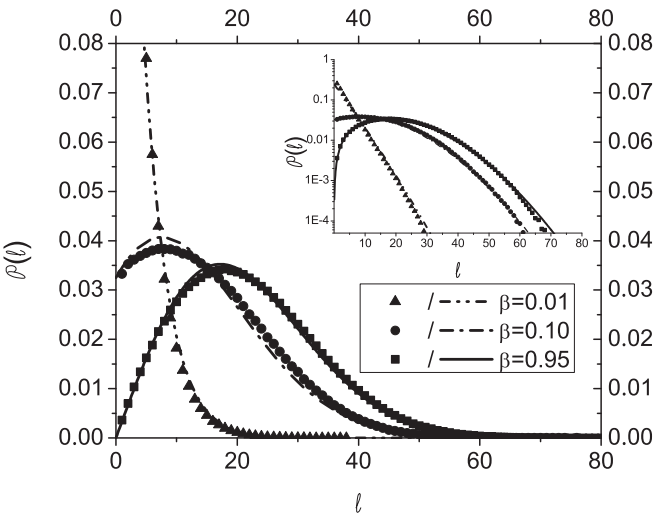

FIG. 2. Gap length distribution between the particles RMA and LMB, $\mathcal{P}(\ell)$. The inset shows the behavior of the distribution for large values of ℓ.

we have

$$p_\delta(x_\alpha) = \int_{-\infty}^{\infty} dx_\gamma \, p(x_A, x_B), \tag{19}$$

with $\delta = A$ and $\gamma = B$ or $\delta = B$ and $\gamma = A$. In the RL regime $p_\delta(x_\delta)$ reduces to the simple expression

$$p_\alpha(x_\delta) = \frac{J}{k} e^{\frac{J(J \pm 2ak\,x_\delta)}{ak^2}} \operatorname{erfc}\left(\frac{J \pm ak\,x_\delta}{\sqrt{a}\,k}\right), \tag{20}$$

where the upper sign corresponds to $\alpha = A$ and the lower to $\delta = B$. Unfortunately, Eq. (17) leads to a lengthy expression for $p_\delta(x_\delta)$ in the DL regime, which we omit for simplicity. However, the average values of x_A and x_B for arbitrary parameter values can be calculated. We found

$$\langle x_\alpha \rangle = \mp \frac{1}{2}\sqrt{\frac{\pi D}{J}} e^{\frac{DJ}{k^2}} \operatorname{erfc}\left(\frac{\sqrt{JD}}{k}\right). \tag{21}$$

For the DL regime, the right side of Eq. (21) reduces to $\mp\sqrt{\pi D/4J}$, while for the RL regime it becomes zero. As a result, we can expect the overlapping of the distributions $p_A(x_A)$ and $p_B(x_B)$ to increase as the value of k decreases. The maximum difference, $\langle x_B - x_A \rangle$, is found in the DL regime and is given by $\sqrt{\pi D/J}$.

The behavior of the marginal distributions $p_A(x)$ and $p_B(x)$ for $\beta = 0.01$ and 0.95 is shown in Fig. 3, where lines correspond to the results obtained from Eq. (19) and dots to the results from kMC simulations. As before, square dots correspond to the DL regime ($\beta = 0.95$) and triangular dots for the RL regime ($\beta = 0.01$). Black and red are used for the distributions of the LMB and RMA particles, respectively. As predicted by our analytical results, in the DL regime, the difference $\langle x_B - x_A \rangle$ is much larger than that in the RL regime. Both distributions have similar mean values in the latter regime, thus $p_A(x_A)$ and $p_B(x_B)$ almost completely overlap. For the parameters used in Fig. 3, Eq. (21) gives $\langle \ell \rangle = \langle x_B - x_A \rangle \approx 23$ for the DL regime, while for the RL regime $\langle \ell \rangle \approx 3.9$. The analytical results given by Eq. (17) agree with the numerical results especially for the RL regime. Because

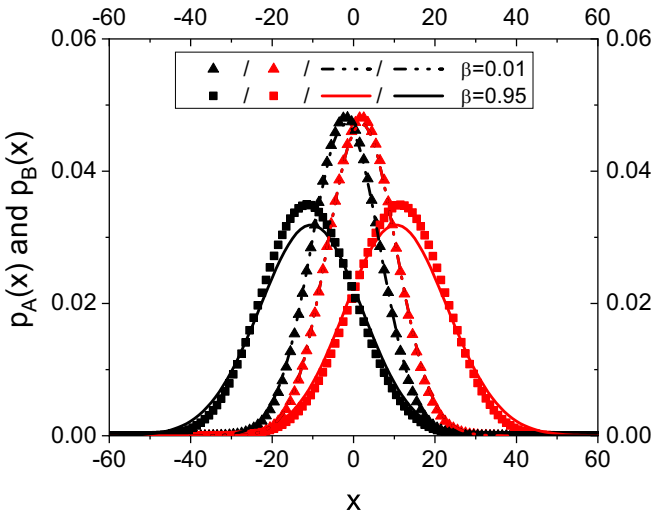

FIG. 3. Marginal distributions $p_A(x)$ and $p_B(x)$. The approximation used to write Eq. (16) works better for the RL regime than in the DL regime.

the RMA and LMB particles can survive close to each other for a long time at low reaction rates, their adjacent particles can populate the sites near the center of the system, confining the RMA and LMB particles. In this sense, in the RL regime the system is more mixed than in the DL regime.

The probability distribution for the position of reactions, $\mathcal{R}(x)$, is shown in Fig. 4. We use square dots for $\beta = 0.95$ and triangles for $\beta = 0.01$. A reaction occurs when $x = x_A = x_B$, and, thus by definition, $\kappa = (x_A + x_B)/2 = x$, and $\mathcal{R}(x)$ is closely related to the distribution of the mass center of particles RMA and LMB, $\mathcal{G}(\kappa)$. Due to the Gaussian nature of $\mathcal{G}(\kappa)$ and the symmetry of the system we expect that $\mathcal{R}(x)$ follows a Gaussian with mean value zero

$$\mathcal{R}(x) = \sqrt{\frac{a}{\pi}} e^{-ax^2}. \tag{22}$$

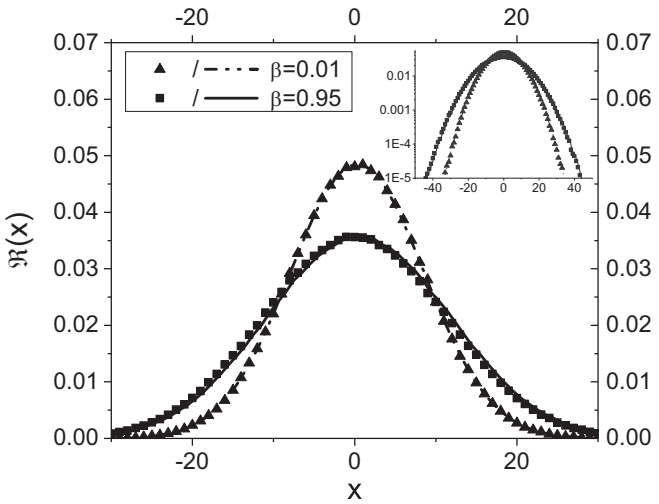

FIG. 4. Probability distributions for the reaction position $\mathcal{R}(x)$. The inset shows the behavior of the distribution for large values of x.

Note that the inset of Fig. 4 supports the validity of this assumption, and Eq. (22) describes quite well the numerical results even for large values of x. We found that $\mathcal{R}(x)$ is wider in the DL regime than in the RL regime, confirming that, as suggested by Fig. 2, in the RL regime the average distance between the RMA and LMB particles is smaller than that in the DL regime. This can be understood considering that in the RL regime, the reaction time is larger than that in the DL regime. In the RL regime, the particles to the left of the RMA particle have more time between consecutive reactions to diffuse to the center of the system, increasing the confinement force on the RMA particle, i.e., increasing the parameter a and the effective external field on the RMA particle. An analogous situation occurs for the LMB particle. The confinement force reduces the available space for the diffusion of the RMA and LMB particles, decreasing the width of the reaction front. With d_p and D held constant, as k decreases, so does the parameter a and the effective quadratic external field, implying that the variances of $\mathcal{R}(x)$ and $\mathcal{G}(\kappa)$ decrease. From our simulations, we found $a \approx 0.0074$ in the RL regime while in the DL regime $a \approx 0.0040$.

Using previous results, it is possible to write an equation for the densities in the steady state. However, we must proceed carefully because the reaction mechanism in the DL regime is quite different from that in the RL regime. Let us consider first the DL regime, for the stationary state we propose

$$\frac{d^2\rho_\delta(x)}{dx^2} = \mathcal{K}\mathcal{F}(x), \tag{23}$$

with $\delta = A$ or B, $\mathcal{K}$ the unknown reaction constant, and $\mathcal{F}(x)$ a function that represents the changes in the densities due to the reactions. In the DL regime, the reactions occur in the low-density region. By definition the density of particles can be calculated from the average $\rho_\alpha(x) = \langle \sum_i \delta(x - x_i) \rangle$ where the sum is extended over all the particles $\alpha = A$ or B. In the case of ρ_A, for $x \gg 0$ the leading term on the average is due to the RMA particle, while for $x \ll 0$, ρ_B is dominated by the contribution of the LMB particle. For densities much smaller than one, $\rho_A(x) \approx p_A(x)$ and $\rho_B(x) \approx p_B(x)$. Therefore, it is reasonable to expect that $\mathcal{F}(x) \propto \mathcal{R}(x) \propto \rho_A(x)\rho_B(x)$. In order to solve the resulting differential equations it is convenient to introduce the auxiliary densities $\rho_+(x) = \rho_A(x) + \rho_B(x)$ and $\rho_-(x) = \rho_A(x) - \rho_B(x)$. The differential equations for $\rho_+(x)$ and $\rho_-(x)$ are

$$\frac{d^2\rho_+(x)}{dx^2} = 2\mathcal{K}\mathcal{R}(x) \quad \text{and} \quad \frac{d^2\rho_-(x)}{dx^2} = 0, \tag{24}$$

respectively. Integrating Eqs. (24) over the interval $[-L, L]$ yields the following result:

$$\left.\frac{d\rho_+}{dx}\right|_{x=L} - \left.\frac{d\rho_+}{dx}\right|_{x=-L} = 2\mathcal{K}, \tag{25}$$

where the limits of the integral over $\mathcal{R}(x)$ were extended over all the real axis because the reactions occur in a region with a length much smaller than $2L$. In the left side of Eq. (25), the first term is J/D, and the second is $-J/D$. Therefore, the reaction constant is given by $\mathcal{K} = J/D$. Figure 5 shows the behavior of the second derivative of the functions $\rho_+(x)$ and $\rho_-(x)$; continuous lines correspond to Eq. (24) and black dots

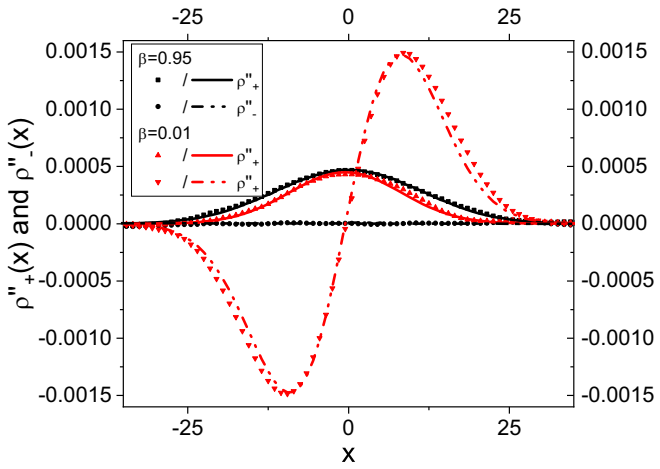

FIG. 5. Reaction kernels for the DL and RL regimes. The behavior of the kernel strongly depends on the regime.

to numerical results for $\beta = 0.95$. The agreement is excellent for both functions. The second derivative of $\rho_-(x)$ is equal to zero, thus, $\rho_-(x)$ must be a linear function of x.

Integrating Eq. (24) it is possible to find

$$\rho_+(x) = \mathcal{K}\, x\, \mathrm{erf}(\sqrt{a}x) + \frac{\mathcal{K}\, e^{-ax^2}}{\sqrt{a\,\pi}} + c_1\, x + c_2 \tag{26}$$

and

$$\rho_-(x) = c_3\, x + c_4, \tag{27}$$

where erf is the error function and the constants c_i are determined by the boundary conditions of the densities $\rho_A(-L) = \rho_B(L) = 1$ and $d\rho_A/dx|_{x=-L} = -d\rho_B/dx|_{x=L} = -J/D$. Thus, for the DL regime we found

$$\rho_\delta(x) = \frac{1}{2}\Bigg[\mathcal{K}\, x\, \mathrm{erf}(\sqrt{a}\, x) + \frac{\mathcal{K}\, e^{-ax^2}}{\sqrt{\pi\, a}} + c_2 + c_1\, x \mp \frac{J(L+x)}{D} \pm 1\Bigg], \tag{28}$$

where the upper sign corresponds to $\delta = A$ and the lower to $\delta = B$. The constants c_1 and c_2 are given by

$$c_1 = \frac{D - JL}{DL} \tag{29}$$

and

$$c_2 = 2 - \mathcal{K}\, L\, \mathrm{erf}(\sqrt{a}\, L) - \frac{\mathcal{K}\, e^{-a\,L^2}}{\sqrt{a\,\pi}} - \frac{JL}{D}. \tag{30}$$

The case of the RL regime is quite different. In this case the reaction does not occur exclusively in the low-density region, and the changes in the densities are not well described by $\mathcal{R}(x)$. Figure 5 shows that, in contrast with the DL regime, for the RL regime (red lines and dots) the reaction kernel is not equal for both species. In order to understand this result we have to take into account that reactions close to but at the left of $x = 0$ increase the flux of particles A because the gap between the RMA and LMB particles will be more likely filled by A particles than by B particles. Similar behavior is found in the region close to but at the right of the center of the system; in this region, the current of A particles decreases while that of B particles increases due to the reactions. This analysis suggests that for $x \ll 0$ we have $\mathcal{F}_A(x) \approx (1-\alpha)p_A(x) < 0$ while for $x \gg 0$ $\mathcal{F}_A(x) \approx (1+\alpha)p_B(x) > 0$ with $\alpha > 1$ a constant. The reaction kernel can be written as a function of the marginal distributions $p_\delta(x_\delta)$; we propose

$$\mathcal{F}_\gamma(x) = (1-\alpha)p_\gamma(x) + (1+\alpha)p_\delta(x), \tag{31}$$

where $\gamma = A$ and $\delta = B$ or $\gamma = B$ and $\delta = A$. Using Eq. (31) in Eq. (23), the auxiliary functions $\rho_-(x)$ and $\rho_+(x)$ satisfy

$$\frac{d^2\rho_+(x)}{dx^2} = \mathcal{K}[p_B(x) + p_A(x)] \tag{32}$$

and

$$\frac{d^2\rho_-(x)}{dx^2} = \alpha\, \mathcal{K}[p_B(x) - p_A(x)]. \tag{33}$$

Figure 5 shows the comparison between the numerical results (red dots) and the analytical approximation (red lines) for the reaction kernel with $\beta = 0.01$. The integration of Eqs. (32) and (33) then leads to

$$\begin{aligned}\rho_+(x) = 1 &- \frac{J(L+x)}{D} \\ &+ \frac{\mathcal{K}\left(-e^{-a\,\xi_1^2} - e^{-a\,\xi_2^2} + e^{-a\,\xi_3^2} + e^{-a\,\xi_4^2}\right)}{2\sqrt{a\,\pi}} \\ &- \frac{\mathcal{K}}{2}\xi_4[\mathrm{erf}(\sqrt{a}\,\xi_1) - \mathrm{erf}(\sqrt{a}\,\xi_4)] \\ &+ \frac{\mathcal{K}}{2}\xi_3[\mathrm{erf}(\sqrt{a}\,\xi_2) + \mathrm{erf}(\sqrt{a}\,\xi_3)]\end{aligned} \tag{34}$$

and

$$\begin{aligned}\rho_-(x) = 1 &- \frac{J(L+x)}{\mathrm{D}} \\ &+ \frac{\alpha\mathcal{K}\left(e^{-a\,\xi_1^2} - e^{-a\,\xi_2^2} + e^{-a\,\xi_3^2} - e^{-a\,\xi_4^2}\right)}{2\sqrt{a\,\pi}} \\ &+ \frac{\alpha\,\mathcal{K}}{2}\xi_3[\mathrm{erf}(\sqrt{a}\,\xi_2) + \mathrm{erf}(\sqrt{a}\,\xi_3)] \\ &+ \frac{\alpha\,\mathcal{K}}{2}\xi_4[\mathrm{erf}(\sqrt{a}\,\xi_1) - \mathrm{erf}(\sqrt{a}\,\xi_4)],\end{aligned} \tag{35}$$

where $\xi_1 = \mu - L$, $\xi_2 = \mu + L$, $\xi_3 = x - \mu$ and $\xi_4 = \mu + x$. The parameter α can be calculated with either of the conditions $\rho_A(-L) = \rho_B(L) = 1$. We found

$$\alpha = \frac{\sqrt{a\,\pi}\, e^{a\,\xi_2^2}[2 - \mathcal{K}Lf(L)]}{\mathcal{K}\left[\sqrt{a\,\pi}\,\mu\, e^{a\,\xi_2^2} f(L) - e^{4\,a\,L\,\mu} + 1\right]}, \tag{36}$$

where

$$f(L) = \mathrm{erf}(\sqrt{a}\,\xi_2) - \mathrm{erf}(\sqrt{a}\,\xi_1). \tag{37}$$

As in the DL regime, the boundary conditions determine the constants of integration. The explicit expressions for the densities are obtained from Eqs. (34) and (35) and taking into account that $\rho_A(x) = (\rho_+(x) + \rho_-(x))/2$ and $\rho_B = (\rho_+(x) - \rho_-(x))/2$.

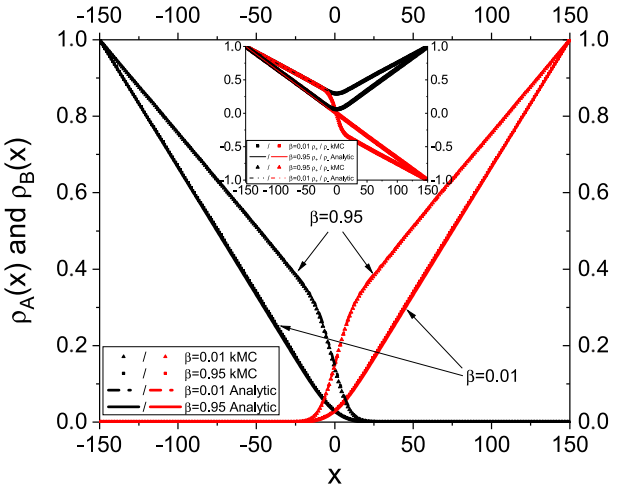

FIG. 6. Density of particles $\rho_A(x)$ and $\rho_B(x)$.

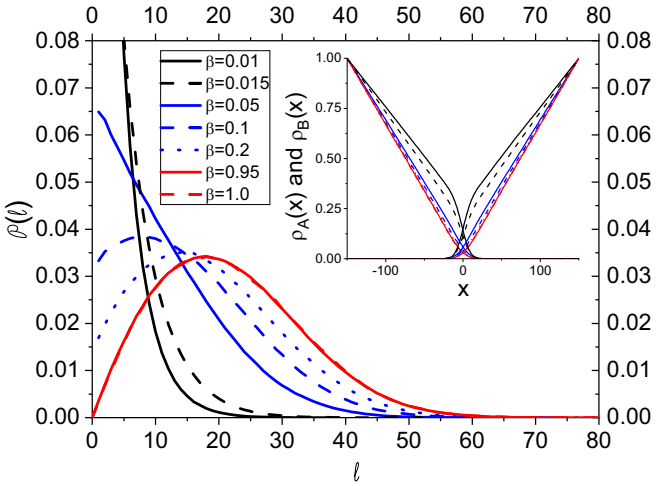

FIG. 7. Gap length distribution and density of particles $\rho_A(x)$ and $\rho_B(x)$ for $d_p = 1$, $\lambda = 0.5$, and different values of β.

The behavior for the density of particles is shown in Fig. 6 for $\beta = 0.01$ and 0.95. Square symbols represents $\beta = 0.95$ and triangular symbols $\beta = 0.01$; black represents the B particles and red A particles. The agreement of our analytical model with the kMC results is excellent. Near the ends of the system, there are no reactions, and the densities satisfy the diffusion equation. Therefore, in the steady state, the density of particles satisfies $d\rho_\alpha/dx = \mp J/D$ and ρ_α behaves linearly close to the ends of the system. The slope J/D allows one to calculate the current J; we found the approximate values of 0.003 and 0.0025 for the DL and RL regimes, respectively. The linear behavior of the densities changes close to the center of the system due to the reactions between A and B particles. The region where the densities do not behave linearly defines the width of the reaction front. The behavior of the auxiliary densities is shown in the inset of Fig. 6. Note that $\rho_+(x)$ has a similar functional form in both regimes, while $\rho_-(x)$ is linear for the DL regime and close to a piecewise linear function for the RL regime. Additionally, in the DL regime, the current of particles behaves monotonically but in the RL regime it does not.

Finally, it is worth showing that, for $d_p = 1.0$, the crossover between DL and RL regimes is characterized by a smooth change of $\mathcal{P}(\ell)$ from the form given by Eq. (2) to that of Eq. (3); see Fig. 7. In contrast, as β increases, the densities $\rho_A(x)$ and $\rho_B(x)$ quickly change from the RL to the DL form. For instance, as shown in Fig. 7 from $\beta > 0.05$ the densities almost have the characteristic shape of the DL regime; however, for $\beta = 0.05$, $\beta = 0.1$, and $\beta = 0.2$ the distribution $\mathcal{P}(\ell)$ clearly differs from Eq. (2). This suggests that the distribution $\mathcal{P}(\ell)$ is more sensitive to the system parameters than the densities and therefore is a better indicator of the regime of the system. Values of β close enough to one guarantee that the system is the DL regime as shown in Fig. 7 where the curves for $\beta = 0.95$ and $\beta = 1.0$ are almost indistinguishable. Similarly, for values of β close to zero the system is in the RL regime. Unfortunately, it is not easy to obtain analytical expressions for $\rho_A(x)$ and $\rho_B(x)$ in the intermediate regime. The general functional form of the reaction kernel for arbitrary values of β remains unknown.

V. CONCLUSIONS

The behavior of the system strongly depends on the ratio between the different timescales of the system. In the DL regime, the diffusion time is much larger than the reaction time, while in the RL the opposite occurs. The difference between both regimes becomes evident when comparing the behavior of the densities $\rho_A(x)$ and $\rho_B(x)$ or the distribution $\mathcal{P}(\ell)$.

Although the reaction is localized in the central region of the system, it affects the density profile in the entire system. This suggests the existence of strong correlations between the position of the particles

The probability to have a reaction at the position x, $\mathcal{R}(x)$, has a Gaussian form in both regimes, but it is wider in the DL than in the RL regime. This is due to the confinement force on the RMA and LMB applied by their neighbors. In the RL regime the marginal distributions $p_A(x)$ and $p_B(x)$ are more overlapped than in the DL regime. Therefore, in the RL regime, the system is more mixed than in the RL regime.

For both regimes, we find expressions for $\rho_A(x)$ and $\rho_B(x)$ which describe well the numerical results. The behavior of these densities were calculated from the reaction kernel $\mathcal{F}(x)$ whose functional form is radically different in both regimes. In the DL regime $\mathcal{F}(x)$ is proportional to $\mathcal{R}(x)$, i.e., it depends on the probability of having the RMA and LMB particles in adjacent sites. However, in the RL regime, the reaction kernel can be approximated by a linear superposition of $p_A(x)$ and $p_B(x)$. For both regimes the reaction kernels can be approximated using the information provided by the distribution $p(x_A, x_B)$, i.e., the reaction kernel can be characterized by this distribution and used to describe the density of particles in the entire system.

Unfortunately, our results cannot be easily extrapolated to quantum systems because quantum effects modify the behavior of these kinds of systems. For example, the results presented in Ref. [24] suggest that the coagulation and annihilation processes do not belong to the same universality class in contrast with their classical counterpart. In future work, it would be interesting to study the system discussed

in this paper but now including quantum effects. For this purpose, the diffusion can be modeled by coherent hopping of hard core bosons while reactions between particles add to the Hamiltonian a dissipative term; see Ref. [21]. In this case we can expect a slower relaxation towards the steady state than that found in the classical system. In general, due to the complexity of the numerical simulation of many-body quantum systems, we know very little about the impact of quantum effects on the dynamical behavior of those systems. Another direct extension of our work is the study of two coupled networks with initially separated reactants. It is well known that the physical properties of RD systems depend on the dimension of the system d due to the properties of random walks depend on d. Therefore, for two coupled networks we can expect new features because the diffusion of particles strongly depends on the topology of the networks.

Binary reaction kinetics in one-dimensional systems can be studied using a thin capillary tube; see Refs. [36–38]. The reaction can be modeled using suitable chemical compounds, for instance, Cr^{3+} for A and xylenol orange (XO) for B or equivalently Cu^{2+} and tetra [disodium ethyl bis-(5-tetrazolylazo) acetate trihydrate]. The kinetics of the front formed in the reaction-diffusion process and the position of the reaction can be monitored by using a CCD camera [38]. In this way it would be possible to archive experimental observations of the quantities calculated in this work.

ACKNOWLEDGMENT

D.L.G. and S.J.V.U. are thankful for the support from Vicerrectoría de Investigaciones to the research project CI 71303, Universidad del Valle (Colombia).

APPENDIX A: DERIVATION OF THE MASTER EQUATION FOR $P_{n,m}(t)$

The general form of the master equation is

$$P_{i,j}(t+\Delta t) = \sum_{\mathcal{C}'} P(\mathcal{C}')\, W_{\mathcal{C},\mathcal{C}'}, \tag{A1}$$

where $W_{\mathcal{C},\mathcal{C}'}$ is the conditional probability to move from configuration $\mathcal{C}'$ to $\mathcal{C}$. The probability $P_{n,m}(t)$ is the probability to have the configuration

$$\mathcal{C}_0: \quad \overset{n}{\bullet}\circ\cdots\circ\overset{m}{\blacktriangle}. \tag{A2}$$

For the sake of simplicity, we consider separately the effect on $P_{n,m}(t)$ due to diffusion and reaction. Let's consider the effect of diffusion. For $m > n+1$, all the configurations with the RMA and LMB at positions n and m, respectively, are

$$\begin{aligned}
C_1:&\quad \circ\overset{n}{\bullet}\circ\cdots\circ\overset{m}{\blacktriangle}\circ,\\
C_2:&\quad \bullet\bullet\circ\cdots\circ\blacktriangle\circ,\\
C_3:&\quad \circ\bullet\circ\cdots\circ\blacktriangle\blacktriangle,\\
C_4:&\quad \bullet\bullet\circ\cdots\circ\blacktriangle\blacktriangle.
\end{aligned}$$

The conditional probabilities to remain in these configurations in a time interval Δt are

$$\begin{aligned}
W_{\mathcal{C}_1,\mathcal{C}_1} &= 1-4\lambda\Delta t,\\
W_{\mathcal{C}_2,\mathcal{C}_2} &= 1-3\lambda\Delta t,\\
W_{\mathcal{C}_3,\mathcal{C}_3} &= 1-3\lambda\Delta t,\\
W_{\mathcal{C}_4,\mathcal{C}_4} &= 1-3\lambda\Delta t.
\end{aligned} \tag{A3}$$

On the other hand, the configurations from where it is possible to reach the configuration $\mathcal{C}_0$ are

$$\begin{aligned}
C_5:&\quad \circ\overset{n+1}{\bullet}\circ\cdots\circ\overset{m}{\blacktriangle},\\
C_6:&\quad \overset{n}{\bullet}\circ\cdots\circ\overset{m-1}{\blacktriangle}\circ,\\
C_7:&\quad \overset{n-1}{\bullet}\circ\cdots\circ\overset{m}{\blacktriangle},\\
C_8:&\quad \overset{n}{\bullet}\circ\cdots\circ\overset{m+1}{\blacktriangle}.
\end{aligned}$$

The conditional probability to reach $\mathcal{C}_0$ in an interval of time Δt for each of these configurations is $\lambda\Delta t$. The change of $P_{n,m}(t)$ due to a reaction can be determined considering the following configuration:

$$C_9: \quad \overset{n}{\bullet}\circ\cdots\circ\overset{k}{\bullet}\overset{k+1}{\blacktriangle}\circ\cdots\circ\overset{m}{\blacktriangle},$$

where conditional probability $W_{\mathcal{C}_0,\mathcal{C}_9} = \beta\Delta t$. Therefore, the change in $P_{n,m}(t)$ due to diffusion and reaction can be written as

$$\begin{aligned}
\frac{dP_{n,m}(t)}{dt} &= -4\lambda P_{n,m}(t) + \lambda[P_{n+1,m}(t) + P_{n-1,m}(t)]\\
&\quad + \lambda\big[P_{n,jm+1}(t) + P_{n,m-1}(t)\big]\\
&\quad + \sum_{k=i+1}^{m-2} P\big(\overset{n}{\bullet}\circ\cdots\circ\overset{k}{\bullet}\overset{k+1}{\blacktriangle}\circ\cdots\circ\overset{m}{\blacktriangle}\big)\\
&\quad - \lambda\, P\big(\overset{n}{\bullet}\circ\cdots\circ\overset{m-1}{\blacktriangle}\blacktriangle\big)\\
&\quad + \lambda\, P\big(\bullet\overset{n}{\bullet}\circ\cdots\circ\overset{m}{\blacktriangle}\big)\\
&\quad - \lambda\, P\big(\bullet\overset{n+1}{\bullet}\circ\cdots\circ\overset{m}{\blacktriangle}\big)\\
&\quad + \lambda\, P\big(\overset{n}{\bullet}\circ\cdots\circ\overset{m}{\blacktriangle}\blacktriangle\big),
\end{aligned} \tag{A4}$$

where $P(\mathcal{C})$ is the probability of the configuration $\mathcal{C}$. It is convenient to define the conditional probabilities $\mathcal{Q}_{n,m}$, $\tilde{\mathcal{Q}}_{n,m}$, and $\mathcal{T}_{n,m,k}$ according to

$$\mathcal{Q}_{n,m} = P\big(\overset{n}{\bullet}\circ\cdots\circ\overset{m}{\blacktriangle}\blacktriangle\big)/P_{n,m}, \tag{A5}$$

$$\tilde{\mathcal{Q}}_{n,m} = P\big(\bullet\overset{n}{\bullet}\circ\cdots\circ\overset{m}{\blacktriangle}\big)/P_{n,m}, \tag{A6}$$

and

$$\mathcal{T}_{n,m,k} = P\big(\overset{n}{\bullet}\circ\cdots\circ\overset{k}{\bullet}\overset{k+1}{\blacktriangle}\circ\cdots\circ\overset{m}{\blacktriangle}\big)/P_{k,k+1}, \tag{A7}$$

respectively. Using these definitions, Eq. (A4) can be written as Eq. (4).

APPENDIX B: kMC ALGORITHM

The events that change the state of the nth site of the lattice ($-N < n < N$) are shown in Table I. All these events depends on the state of the sites $n-1$ and $n+1$. Note that some configurations such as the one of the first row has associated two different processes, while other such as the ones in the third column have just one. Notice that in this procedure we have taken $\beta/2$ to eliminate the double counting of the reaction events.

The cases of $n = -N$ and $n = N$ is different not only due to the deposition but also because these sites just have one nearest neighbor instead of two. For these cases we have the events shown in Table II. The catalog of the

TABLE I. Catalog of the events that change the state of the nth site of the lattice.

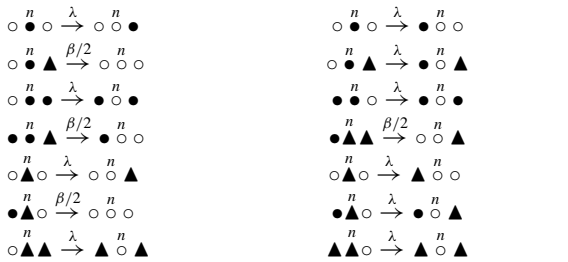

TABLE II. Catalog of the events that change the state of the sites $-N$ and N of the lattice.

events defines the number N_k of transitions in the system and their associated rates r_k. The total rate $R_k = \sum_{i=1}^{N_k}$ is the sum of the rates of all possible transitions. The algorithm is the following. At each time step all the possible transitions are determined and the total rate is calculated. A random number $r \in [0, R_k]$ is generated. This number determines the transition d_p selected according to $\sum_{i=1}^{j-1} < r < \sum_{i=1}^{j+1}$. The time is advanced according to $\Delta t = -R_k^{-1} \log(r)$. This procedure is repeated for each time step.

[1] A. M. Turing, The chemical basis of morphogenesis, Phil. Trans. R. Soc. Lond. B **237**, 37 (1952).

[2] M. J. E. Richardson, Exact solution of two-species ballistic annihilation with general pair-reaction probability, J. Stat. Phys. **89**, 777 (1997).

[3] M. Küntz and P. Lavallée, Anomalous diffusion is the rule in concentration-dependent diffusion processes, J. Phys. D: Appl. Phys. **37**, L5 (2004).

[4] A. N. Landge, B. M. Jordan, X. Diego, and P. Müller, Pattern formation mechanisms of self-organizing reaction-diffusion systems, Dev. Biol. **460**, 2 (2020).

[5] H. Simon, Concentration for one and two-species one-dimensional reaction-diffusion systems, J. Phys. A: Math. Gen. **28**, 6585 (1995).

[6] S. Subramanian and S. M. Murray, Pattern selection in reaction diffusion systems, Phys. Rev. E **103**, 012215 (2021).

[7] D. ben-Avraham and S. Havlin, *Diffusion and Reactions in Fractals and Disordered Systems* (Cambridge University Press, Cambridge, 2000).

[8] P. Krapivsky, S. Redner, and E. Ben-Naim, *A Kinetic View of Statistical Physics* (Cambridge University Press, Cambridge, 2010).

[9] D. Zhong and D. Ben-Avraham, Diffusion-limited coalescence with finite reaction rates in one dimension, J. Phys. A: Math. Gen. **28**, 33 (1995).

[10] D. L. González and G. Téllez, The crossover between organized and disorganized states in some nonequilibrium systems, J. Phys. A: Math. Theor. **42**, 195001 (2009).

[11] M. Hoyuelos, H. O. Martin, and E. V. Albano, Study of the steady state of a two-species annihilation process with separated reactants, J. Phys. A: Math. Gen. **28**, L483 (1995).

[12] M. Hnatich, J. Honkonen, and T. Lučivjanský, Study of anomalous kinetics of the annihilation reaction $A + A \to \emptyset$, Theor. Math. Phys. **169**, 1481 (2011).

[13] P. Oliva and D. H. Zanette, Reaction kinetics of annihilating particles with anomalous diffusion, Phys. Rev. E **51**, 6258 (1995).

[14] D. Toussaint and F. Wilczek, Particle-antiparticle annihilation in diffusive motion, J. Chem. Phys. A. **78**, 2642 (1983).

[15] P. Argyrakis and R. Kopelmann, Nearest-neighbor distance distributions and self-ordering in diffusion-controlled reactions. II. A+B simulations, Phys. Rev. A **41**, 2121 (1990).

[16] P. Argyrakis and R. Kopelman, Nearest-neighbor distance distributions and self-ordering in diffusion-controlled reactions. I. A + A simulations, Phys. Rev. A **41**, 2114 (1990).

[17] M. Catanzaro, M. Boguñá, and R. Pastor-Satorras, Diffusion-annihilation processes in complex networks, Phys. Rev. E **71**, 056104 (2005).

[18] G. Cencetti, P. Clusella, and D. Fanelli, Pattern invariance for reaction-diffusion systems on complex networks, Sci. Rep. **8**, 16226 (2018).

[19] T. Emmerich, A. Bunde, and S. Havlin, Diffusion, annihilation, and chemical reactions in complex networks with spatial constraints, Phys. Rev. E **86**, 046103 (2012).

[20] F. Lazaridis, B. Gross, M. Maragakis, P. Argyrakis, I. Bonamassa, S. Havlin, and R. Cohen, Spontaneous repulsion in the $A + B \to 0$ reaction on coupled networks, Phys. Rev. E **97**, 040301(R) (2018).

[21] M. van Horssen and J. P. Garrahan, Open quantum reaction-diffusion dynamics: Absorbing states and relaxation, Phys. Rev. E **91**, 032132 (2015).

[22] C. D. Greenman, Reaction diffusion systems and extensions of quantum stochastic processes, J. Phys. A: Math. Theor. **56**, 235002 (2023).

[23] S. R. Dahmen, Reaction-diffusion processes described by three-state quantum chains and integrability, J. Phys. A: Math. Gen. **28**, 905 (1995).

[24] G. Perfetto, F. Carollo, J. P. Garrahan, and I. Lesanovsky, Reaction-Limited Quantum Reaction-Diffusion Dynamics, Phys. Rev. Lett. **130**, 210402 (2023).

[25] K. Kang and S. Redner, Scaling Approach for the Kinetics of Recombination Processes, Phys. Rev. Lett. **52**, 955 (1984).

[26] E. Ben-Naim and S. Redner, Inhomogeneous two-species annihilation in the steady state, J. Phys. A: Math. Gen. **25**, L575 (1992).

[27] L. Gálfi and Z. Rácz, Properties of the reaction front in an $A + B \to C$ type reaction-diffusion process, Phys. Rev. A **38**, 3151 (1988).

[28] H. Taitelbaum, Segregation in reaction-diffusion systems, Physica A **200**, 155 (1993).

[29] Z. Jiang and C. Ebner, Simulation study of reaction fronts, Phys. Rev. A **42**, 7483 (1990).

[30] F. Leyvraz and S. Redner, Spatial Organization in the Two-Species Annihilation Reaction $A + B \to 0$, Phys. Rev. Lett. **66**, 2168 (1991).

[31] S. B. Yuste, L. Acedo, and K. Lindenberg, Reaction front in an $A + B \to C$ reaction-subdiffusion process, Phys. Rev. E **69**, 036126 (2004).

[32] D. Ben-avraham, The method of inter-particle distribution functions for diffusion-reaction systems in one dimension, Mod. Phys. Lett. B **9**, 895 (1995).

[33] M. Andersen, C. Panosetti, and K. Reuter, A practical guide to surface kinetic Monte Carlo simulations, Front. Chem. **7**, 202 (2019).

[34] A. F. Voter, Introduction to the kinetic Monte Carlo method, in *Radiation Effects in Solids*, edited by K. E. Sickafus, E. A. Kotomin, and B. P. Uberuaga (Springer, Netherlands, Dordrecht, 2007), pp. 1–23.

[35] T. Oppelstrup, V. V. Bulatov, A. Donev, M. H. Kalos, G. H. Gilmer, and B. Sadigh, First-passage kinetic Monte Carlo method, Phys. Rev. E **80**, 066701 (2009).

[36] Y. E. L. Koo and R. Kopelman, Space-and time-resolved diffusion-limited binary reaction kinetics in capillaries: Experimental observation of segregation, anomalous exponents, and depletion zone, J. Stat. Phys. **65**, 893 (1991).

[37] H. Taitelbaum, B. Vilensky, A. Lin, A. Yen, Y.-E. Lee Koo, and R. Kopelman, Competing Reactions with Initially Separated Components, Phys. Rev. Lett. **77**, 1640 (1996).

[38] S. H. Park, S. Parus, R. Kopelman, and H. Taitelbaum, Gel-free experiments of reaction-diffusion front kinetics, Phys. Rev. E **64**, 055102(R) (2001).